IEEE Access
The journal for rapid open access publishing

Received October 10, 2014, accepted October 16, 2014, date of publication October 20, 2014, date of current version October 30, 2014.

Digital Object Identifier 10.1109/ACCESS.2014.2364091

Deep-Subwavelength MIMO Using Graphene-Based Nanoscale Communication Channel

SHINYA SUGIURA[1], (Senior Member, IEEE), AND HIDEO IIZUKA[2], (Member, IEEE)
[1]Department of Computer and Information Sciences, Tokyo University of Agriculture and Technology, Tokyo 184-8588, Japan
[2]Toyota Central Research and Development Laboratories, Inc., Aichi 480-1192, Japan

Corresponding author: S. Sugiura (sugiura@ieee.org)

ABSTRACT In this paper, a novel graphene-based multiple-input multiple-output (MIMO) concept is proposed for high-rate nanoscale wireless communications between transceivers, which are nano/micrometers apart from each other. In particular, the proposed MIMO architecture considers exploiting a deep-subwavelength propagation channel made of graphene. This allows us to increase the number of transmitted symbol streams, while using a deep-subwavelength arrangement of individual plasmonic nanotransmit/receive elements in which the spacing between the transmitters and/or the receivers is tens of times smaller than the wavelength. This exclusive benefit is achieved with the aid of the phenomenon of graphene plasmons, where graphene offers the extremely confined and low-loss plasmon propagation. Hence, the proposed graphene-based MIMO system is capable of combating the fundamental limitations imposed on the classic MIMO configuration. We also present a novel graphene-specific channel adaptation technique, where the chemical potential of the graphene channel is varied to improve the power of the received signals.

INDEX TERMS Correlation, chemical potential, deep subwavelength, diffraction limit, graphene, MIMO, nanoscale communication, surface plasmon polariton.

I. INTRODUCTION

Recent advances in nanotechnology have enabled the development of nanoscale devices, which are expected to be the most basic units of nanomachines and nanoelectromechanical systems (NEMS) [1]. In order for these devices to accomplish further useful and complex tasks, it is necessary to incorporate a means of communications between them. This emerging research field is referred to as *nano communications* [2]–[5]. Promising applications include biomedical applications operated by *in-vivo* nanomachines, environmental monitoring aided by wireless nanosensor networks, and high-rate interconnects functioning inside computers [6]. For the efficient transmissions of electromagnetic waves, several nanoscale components have been developed, including nanoantennas [7], carbon nanotube (CNT) transceivers [8], [9], self-powered nano-generators [10] and nanoscale field effect transistors (FETs) [11], [12].

Graphene is one of the most promising materials for nanoscale electronics [13], and it has several unique characteristics. In particular, graphene plasmons provide a suitable alternative to metal plasmons, since extreme confinement and relatively long propagation distances are achievable [14]. Furthermore, electrical or chemical modification of the charge-carrier density allows dynamic tuning of the plasmon spectrum. For example, graphene was integrated into the nanogaps of coupled plasmonic antennas in order to achieve broad tuning of antenna resonance [15]. Similarly, in the previous study [16] a nanoantenna was composed of graphene, which is capable of operating at a lower frequency than its metallic counterpart. In [17], a THz beamforming antenna was developed with the aid of a switchable high-impedance surface using a single-layer graphene.

In the field of microwave communications, the multiple-input multiple-output (MIMO) concept [18], [19] has been extensively explored as an enabler of high-speed data transmissions. In MIMO systems, multiple antenna elements are typically utilized both at the receiver and transmitter. Multiple symbols are simultaneously transmitted from the transmit antennas in order to multiplex signals in the spatial dimension. Hence, in a MIMO scheme, an increase in the number of transmit and receive antenna elements allows a linear increase in capacity [20]. Owing to this benefit, the recent

microwave communication standards [21], such as long-term evolution (LTE) and WiMAX, have typically included the MIMO techniques.

In contrast, one of the fundamental limitations of MIMO systems is caused by the array configuration [22], [23]. To be more specific, at both the transmitter and the receiver, the multiple antenna elements must be sufficiently separated such that the channels are uncorrelated. Otherwise the receiver will be unable to decompose and demodulate multiple signals multiplexed in the spatial domain. However, it is typically a challenging task to maintain uncorrelated channel components, i.e., to ensure that the antenna spacing remains larger than the order of one wavelength, especially in a scenario such as a mobile handset or a nano-circuit interconnect. Additionally, the MIMO scheme's achievable performance depends largely on the instantaneous channel conditions, and thus the maximum gain of the MIMO system is not necessarily attainable.

As a way of solving the above-mentioned problem associated with antenna spacing, the concept of subwavelength focusing was used in the design of MIMO communications [24]. In this arrangement, a far-field time-reversal mirror was used to build a time-reversed wave field that interacts with the lossy random medium to regenerate the propagating waves as well as the evanescent waves. Since these waves were designed to refocus below the diffraction limit, a focal spot of one-thirtieth of a wavelength was demonstrated in this arrangement. More recently [25], antenna arrays composed of CNT were utilized for spectrally efficient MIMO transmissions in the terahertz band. In that scheme, the number of antenna arrays per area was designed to optimize the bundle size, while considering the effects of the fabrication tolerance.

Against this background, the novel contribution of this paper is that we propose the concept of graphene-based MIMO communication, where the nanoscale MIMO transmissions are enabled over the graphene-based deep-subwavelength channel. The unique benefits of our arrangement are as follows. The proposed graphene-based MIMO architecture makes it possible to attain the maximum achievable transmission rate, while combating its fundamental limitation of antenna spacing. More specifically, by exploiting the surface plasmon polaritons (SPPs) of a graphene channel, the effective wavelength becomes tens of times shorter than that experienced in free space, while achieving a significantly lower propagation loss than that found in a conventional study [24]. For our proposed system operating at a frequency of 10 THz, the size of a MIMO system is 30 times smaller than one in a conventional system. Furthermore, the gain of the graphene channel can be optimized by adjusting the chemical potential of the graphene. Hence, graphene-specific characteristics provide additional degrees of freedom in the design and contribute to maximizing the achievable rate.[1]

[1]For example, the proposed graphene-based MIMO scheme is useful for the information transfer between nanoscale circuits. However, the potential benefits of our new communication concept are not limited to this, but include many diverse applications in the nanoscale communication field [2], [4], [5].

The remainder of this paper is organized as follows. In Section II we provide an extensive review of related literature. In Section III we propose a novel graphene MIMO architecture and discuss the effects of the SPPs, while in Section IV we discuss the capacity of the proposed scheme as well as the achievable performance. Finally this paper is concluded in Section V.

II. REVIEW OF RELATED WORKS

A. MINIATURIZATION OF MIMO DEVICES

In this section, the literature review is carried out for miniaturization of MIMO devices, especially for those of antenna arrays. The system arrangement of a MIMO system differs depending on the targeted gain attainable by an antenna array. In particular, the functions of MIMO techniques may be classified into four categories [26], [27], i.e., spatial-multiplexing, diversity, beamforming, and space-division multiple-access techniques. As mentioned in Section I, our main focus of this paper is on spatial multiplexing [28], [29], where multiple independent signal substreams are transmitted from different transmit antenna elements at the same frequency and within the same time slot, therefore the corresponding transmission rate is multiplied by the number of transmit antennas.

The capacity of spatial-multiplexing MIMO systems largely depends on the rank of the $(N \times M)$–sized channel matrix [30], where M is the number of transmit antennas and N is the number of receive antennas. More specifically, the MIMO channels are characterized by the fading and correlation properties [31], and hence the propagation channel represents major parameters that impact the achievable system performance. This indicates that a rich multipath environment and a low correlation contribute to the beneficial gains achievable by the MIMO technique [32].

Traditionally in the field of microwave communications, a compact array configuration has been required, since space of a mobile handset is limited. However, antenna elements typically need to be spaced by more than a half wavelength $\lambda_0/2$ in order to have suitable isolation and low correlation between the elements. Here, λ_0 represents a free-space wavelength. Small spacings between the antennas lead to unignorable mutual coupling, which typically reduces the efficiency of the antennas. Consequently, the signal-to-noise ratio (SNR) is degraded and the signals at the antennas are correlated [33]. In order to evaluate the performance of MIMO systems using a compact array, the associated framework, system model and theoretical limit were presented [33], [34]. In particular, a framework to analyze compact arrays for MIMO is presented in [33], where the effects of mutual coupling between small-spacing antennas are taken into account. Furthermore, in [34] the theoretical limitations of densely-packed MIMO antenna elements into small volumes were examined, while considering the area and geometry constraints based on the combination of antenna theory and with observations from spatial channel measurements.

TABLE 1. Contributions to the miniaturization of MIMO array.

Year	Authors	Contribution
2004	Waldschmidt, Schulteis and Wiesbeck [33]	A framework to analyze compact arrays for MIMO was presented, where the effects of mutual coupling between small-spacing antennas are taken into account.
2005	Getu and Andersen [37]	The authors developed a compact cubic-structured array, where the 12 edges consist of electrical dipole antennas. The side length was reduced from $\lambda_0/2$ to $\lambda_0/20$.
2006	Browne, Manteghi, Fitz and Rahmat-Samii [38]	Indoor measurements were carried out in order to characterize and design a compact handset array using a printed-inverted-F antenna. The near independently identically distributed Gaussian capacity for a 4-by-4 MIMO system was observed when the array volume was as small as $0.45\lambda_0 \times 0.12\lambda_0 \times 0.07\lambda_0$.
2007	Lerosey, de Rosny, Tourin and Fink [24]	The antenna spacing of an array was reduced to $\lambda_0/30$ with the aid of subwavelength focusing based on evanescent waves and time-reversal processing.
2008	Volmer *et al.* [42]	In order to investigate the effects of power mismatch imposed by a compact array closer than $\lambda_0/2$, the authors presented the analytical tool based on a superposition of eigenmodes of an array.
2010	Bait-Suwailam, Boybay and Ramahi [39]	Single-negative magnetic metamaterials were used in order to maintain low correlation between the antenna elements of an array.
2011	Lee *et al.* [40]	An antenna array was fabricated on a ferrite substrate for handset terminals, where the separation of the prototype two-element array was as low as $\lambda_0/10$.
2012	Lau and Andersen [41]	The method of decoupling two closely coupled antennas with a parasitic scatterer was proposed in order to achieve a compact MIMO two-monopole array with an antenna spacing of $\lambda_0/10$.

In order to minimize the size of an antenna array of MIMO while maintaining a low antenna correlation and mutual coupling between the antenna elements, the effects of mutual coupling and a matching network on the performance of compact MIMO systems have been investigated [35], [36]. In [35] capacity of MIMO systems with closely spaced antenna elements was investigated. The authors concluded that as the channel-measurement results of 4-by-4 MIMO system at 5.2 GHz, the capacity remains large even if antenna spacing is as low as $\lambda_0/5$. In [36] the effect of matching network on the performance of wide-band MIMO systems was considered.

Moreover, the diverse compact array arrangements have been proposed [24], [37]–[41] and a range of major contributions on the subject of the array miniaturization and related techniques are listed in Table 1. In [37], a cubic structure with integrated planar antenna elements has been developed for MIMO applications, where the cube has many antennas mounted on them, each of which is fed by a different port so that isolation between ports is desirable. In particular, the side length of the antenna array for a spatial-multiplexing MIMO system was reduced to $\lambda_0/20$ from the conventional size of a half-wavelength array $\lambda_0/2$. In [24], the authors proposed subwavelength focusing of independent substreams on different receive antenna elements in the context of indoor MIMO systems. More specifically the random lossy medium is employed near the receive antenna array in order to generate subwavelength evanescent waves. Additionally, far-field time-reversal signal processing is operated for refocusing decomposed signal streams to the receive antennas. Consequently, the resultant antenna spacing is as low as $\lambda_0/30$, although the propagation loss of the evanescent wave is considerably high.

As above-mentioned, the miniaturization factor of the previous compact MIMO arrays was in the range of ten to thirty. In contrast, our proposed graphene-based MIMO concept has the potential of reducing the effective wavelength by the factor of 30 to 100. Hence, a further more compact array configuration is attainable.

B. GRAPHENE PLASMONS

We next present a brief overview of graphene plasmons. Surface plasmons are electromagnetic waves that propagate along the surface of a conductor, conventionally a metal, via the interaction with the free electrons of the conductor [43], [44]. Noble metals such as silver and gold are widely used for the excitation of surface plasmons at a subwavelength scale in the visible and infrared regions. However, the propagation length is limited due to the large ohmic loss and the propagation is hardly tuned.

Graphene is a single layer of carbon atoms in a hexagonal lattice and significant progresses have been made over the past decade to reveal unique properties of graphene and find potential applications since the experimental discovery in 2004 [13]. Charge carriers can travel thousands of interatomic distances without scattering and their motilities exceed 200,000 $\mathrm{cm}^2 \cdot \mathrm{V}^{-1} \cdot \mathrm{s}^{-1}$ [45]–[47]. Graphene may be described as a zero-gap semiconductor and can be doped to high values of carrier concentrations at ambient conditions. Thus, surface plasmons propagating along a graphene layer exhibit the extreme confinement while attaining low-loss propagation. As the result, graphene plasmons accomplish an approximately 10 times more confinement effect and approximately 100 times more propagation length than those of conventional surface plasmon propagations at the silver/silicon interface in the infrared regime [48]. Moreover, graphene plasmons are widely controlled by tuning the chemical potential of graphene. Particularly, external voltage control of the chemical potential enables optoelectronic devices. For example, graphene-based modulators exhibit compact footprint due to the strong interaction with light and ultrafast modulation [49], [50]. Graphene-based field-effect transistors are expected to find radio-frequency

applications due to the extremely thin channel as well as the excellent carrier transport property [51], [52]. In addition, extensive works on efficient photodetectors have been reported [53]–[55].

The optical conductivity ρ of graphene consists of the intraband and interband contributions and is given with the chemical potential μ, as follows [56]:

$$\rho = \frac{i}{\omega + i/\tau}\frac{e^2 2k_bT}{\pi\hbar^2}\ln\left[2\cosh\left(\frac{\mu}{2k_bT}\right)\right] + \frac{e^2}{4\hbar}\left[G\left(\frac{\hbar\omega}{2}\right) + i\frac{4\hbar\omega}{\pi}\int_0^\infty \frac{G(\zeta) - G(\hbar\omega/2)}{(\hbar\omega)^2 - 4\zeta^2}\right], \quad (1)$$

where

$$G(\zeta) = \frac{\sinh(\zeta/k_bT)}{[\cosh(\mu/k_bT + \cosh(\zeta/k_bT))]}, \quad (2)$$

and e is the charge of an electron, k_b is the Boltzmann constant, $\hbar$ is the reduced Planck constant, and ω is the angular frequency.

The graphene plasmon of the free-standing graphene sheet is characterized by the dispersion equation [48]:

$$\frac{2}{\kappa_0} + i\frac{\rho}{\omega\epsilon_0} = 0, \quad (3)$$

where

$$\kappa_0 = \sqrt{\beta^2 - k_0^2} \text{ for } \beta^2 > k_0^2, \quad (4)$$

and β is the lateral wavenumber of graphene plasmons, k_0 is free-space wavenumber, and ϵ_0 is the free-space permittivity. Therefore, (1)–(4) are the fundamental equations, which characterize the graphene channel.

Most recently, it has been discovered that graphene plasmons are highly reflected at the graphene edge [57]. Also, similar characteristics were found to be attained with the aid of graphene gap on a stepped silicon carbide substrate [58], defects [59], and grain boundaries [60]. From the viewpoint of communication application of graphene, this may enable the generation of a rich multipath environment, hence potentially having the merit of attaining an uncorrelated MIMO channel, as mentioned in Section II-A. The proposed graphene-based MIMO system shown in Section III is designed to fully exploit this low-loss reflection effect, in addition to those of the deep subwavelength and the low-loss propagation.

III. MIMO USING GRAPHENE

In this section the schematic of our graphene-based MIMO system is firstly introduced. We then discuss the mechanisms of the deep-subwavelength effects that are specific to graphene in an analytical manner.

A. SYSTEM MODEL

We consider a MIMO system, where ($M = 2$) individual plasmonic nano-sources and ($N = 2$) plasmonic nano-receivers are implemented in order to excite the SPP wave on a single graphene layer, as shown in Fig. 1. For simplicity, we will assume in the analytical model that the plasmonic nano-sources and receivers are infinitesimal and excite graphene plasmons, i.e., ideal point sources, as commonly employed in the related studies [61], [62]. The effects of graphene plasmons allow us to attain the primary advantage of our system: deep-subwavelength scaling in a MIMO system, in which the effective wavelength is tens of times smaller than that in free space. Note that this deep-subwavelength effect varies depending on the chemical potential of the graphene. The graphene plasmons are reflected at the edge of the graphene sheet due to the large impedance mismatch between graphene and air [57]. Graphene plasmons are characterized by low-loss propagation, and our analytical model has a multi-reflection environment. Consequently, the proposed system experiences a sufficiently high number of multi-paths to ensure that the channels are uncorrelated; this is beneficial to a MIMO system. Furthermore, the chemical potential of the graphene can be dynamically tuned by an external voltage source, e.g., between the graphene sheet and the doped silicon substrate, as shown in the inset of Fig. 1. This enables us to adaptively tune the wavelength of the graphene plasmon. Thus, the MIMO system presented here can tune the wavelength in order to avoid the drops in the received power that occur in multi-reflection environments; this is the second advantage of the proposed graphene-based arrangement. In Section IV, free-standing graphene [6] will be used in a numerical investigation of the effectiveness of the MIMO system.

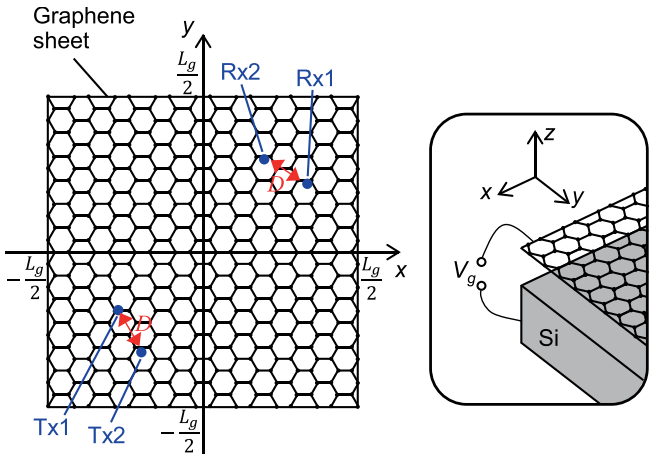

FIGURE 1. Analytic model of a MIMO system, where ($M = 2$) individual plasmonic nano-sources and ($N = 2$) plasmonic nano-receivers are implemented in order to excite the SPP wave on a single graphene layer. In the analytic model, the free-standing graphene sheet is considered. The design frequency is $f_0 = 10$ THz. The four plasmonic nano tranceivers are positioned at (x, y) = (−340, −220), (−250, −400), (420, 280), and (240, 370) (unit: nm) for Transmitter 1, Transmitter 2, Receiver 1, and Receiver 2. The graphene sheet has an area of ($L_g \times L_g$) = 1.2 μm ×1.2 μm and a chemical potential of 0.3 eV. The chemical potential of the graphene can be tuned dynamically by an external voltage between the graphene sheet and the doped silicon substrate as shown in the inset.

B. PROPAGATION CHARACTERISTICS OF GRAPHENE PLASMONS

The graphene plasmons are tightly confined in the graphene layer, as shown in Fig. 2(a); the magnetic field distribution of

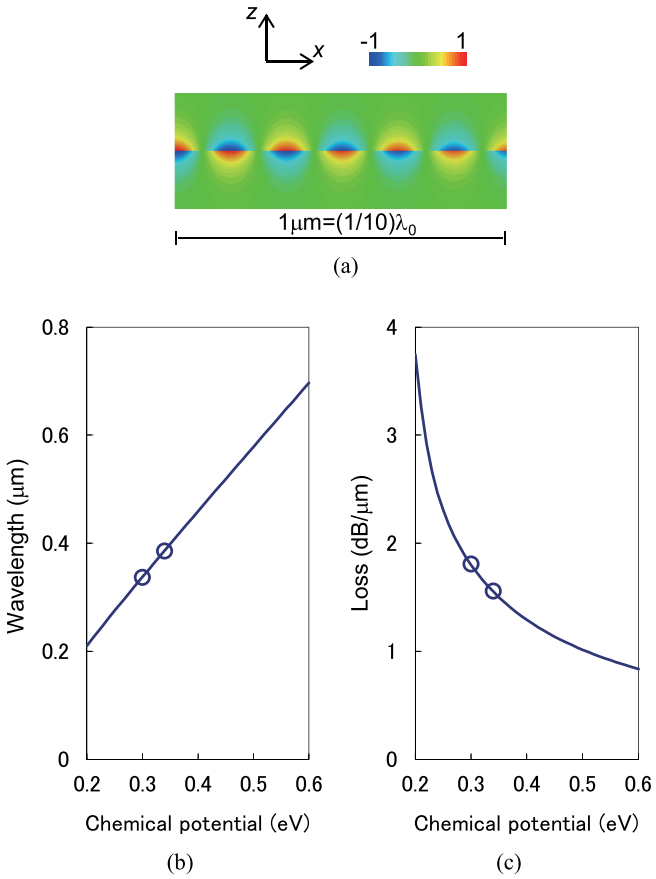

FIGURE 2. **(a) Magnetic field distribution of graphene plasmons propagating along the x axis obtained by the CST Microwave Studio simulation. (b) Wavelength and (c) loss of graphene plasmon propagation. Curves indicate the analytical results based on (3) and symbols indicate the numerical results obtained by the CST Microwave Studio simulations.**

the graphene plasmon propagation was obtained by using the CST Microwave Studio [63]. More specifically, in our simulations, each plasmonic nano-transmitter/receiver is modeled as a line source [61], [62] for the excitation of SPPs. Note that the graphene is modeled as a thin dielectric layer [6]. In (1), we assume that the electron scattering lifetime is $\tau = 0.5$ ps [47], [64], [65], and the temperature is $T = 300$ K. Therefore, the plasmon wavelength is at the deep-subwavelength scale. When the chemical potential is set to 0.3 eV, the plasmon wavelength is $\lambda_{0.3\text{eV}} = 337$ nm at the design frequency of $f_0 = 30$ THz ($\lambda_0 = 10\ \mu$m). This implies that the wavelength is shortened by a factor of $(10 \times 10^{-6})/(337 \times 10^{-9}) \simeq 30$.

The dispersion characteristic is calculated based on (1) and (3) in order to obtain the complex wavenumber β. Figs. 2(b) and (c) show the effective wavelength and the propagation loss, respectively, where the real part of the wavenumber β corresponds to the effective wavelength, while the imaginary part of β represents the propagation loss. We see in Fig. 2(b) that graphene plasmons can be widely tuned by changing the chemical potential. Considering that the corresponding wavelength in free space is $\lambda_0 = 10\ \mu$m, the ratio of the effective wavelength of graphene over λ_0 is from 14 to 50 in the range of chemical potentials shown in Fig. 2(b). Moreover, observe in Fig. 2(c) that graphene plasmons had a low-loss profile, in the range of less than 2 dB/μm, when the chemical potential was higher than 0.3 eV. This is a unique advantage of graphene plasmons, since other deep-subwavelength techniques [24], [66] typically exhibit a higher propagation loss. The numerical results obtained by the CST Microwave Studio (symbols) agreed well with the analytic results (blue lines) in Figs. 2(b) and (c), with chemical potentials of 0.3 eV and 0.34 eV, respectively.

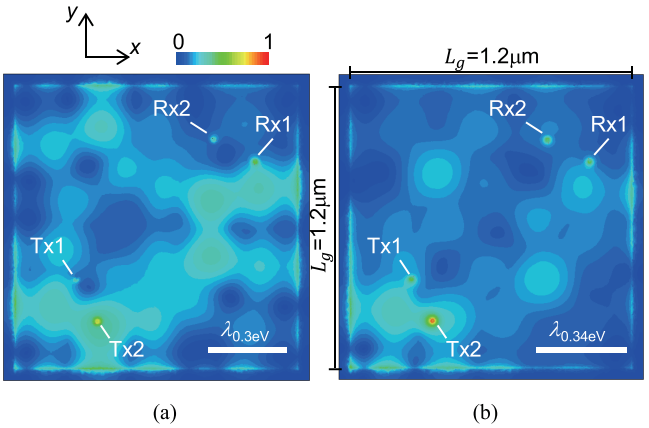

FIGURE 3. **Snap-shots of the distribution of the intensity of the electric field at a distance of 2 nm from the graphene surface with the excitation of graphene plasmons at Transmitter 2. The chemical potentials were (a) 0.3 eV and (b) 0.34 eV.**

In Fig. 3, we present the results of using CST Microwave Studio to numerically investigate the electromagnetic field distributions and scattering parameters of the 2-by-2 MIMO system. We began the investigation with the parameters shown in the caption of Fig. 1. The positions of the two transmit plasmonic nano-sources are given by (x, y) = (−340, −220), (−250, −400), while those of the two plasmonic nano-receivers are (420, 280) and (240, 370). Fig. 3(a) shows the intensity distribution of the electric field at a distance of 2 nm from the graphene surface and with a chemical potential of 0.3 eV. This multi-reflection environment with reflections at the graphene edges results in standing waves. When the chemical potential is varied from 0.3 eV to 0.34 eV, the electric field intensity has a different profile and a longer wavelength of $\lambda_{0.34\text{eV}} = 386$ nm. These results verify the second advantage: nulls in the received power can be avoided by tuning the chemical potential of the graphene. Note that this channel adaptation technique based on varying the chemical potential is not limited to the case of Fig. 3. Rather, it can be readily applied to an arbitrary arrangement of plasmonic nano-transceivers in order to assist in the recovery from fading-induced deterioration.

IV. CAPACITY AND RESULTS

In this section, we evaluate our proposed graphene-based MIMO scheme in terms of channel capacity, which characterizes the maximum achievable limit of a

communication system. Note that channel capacity takes into account the effects of channel correlation in the MIMO systems, hence it is an appropriate performance metric for our graphene-based MIMO scheme capable of solving the problem of a channel correlation. The instantaneous maximum capacity of a MIMO system is given by [22]

$$C_{\mathrm{MIMO}} = \log_2 \left[\det \left(\mathbf{I} + \frac{\gamma}{M} \mathbf{H}\mathbf{H}^H \right) \right], \tag{5}$$

where M is the number of transmit plasmonic nano-sources, γ represents the received SNR, $\mathbf{I} \in \mathbb{R}^{M \times M}$ is the M-size identity matrix, and $\mathbf{H} \in \mathbb{C}^{N \times M}$ is the channel matrix, where the element in the nth-row and the mth column corresponds to the channel coefficient between the mth transmit plasmonic nano-sources and the nth plasmonic nano-receivers. Note that a performance close to this capacity limit (5) is typically achievable when using one of the powerful channel coding schemes [19], such as a turbo code or a low-density parity check (LDPC) code.

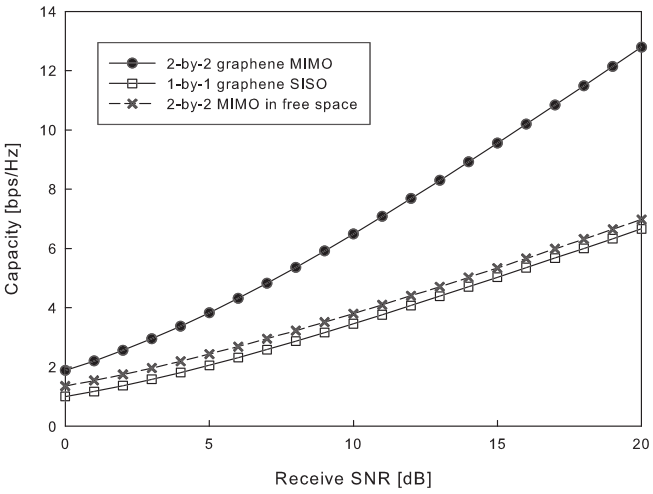

FIGURE 4. Instantaneous maximum capacity of our 2-by-2 graphene-based MIMO system. The system parameters used in the simulations were the same as those in Fig. 3(a). We also plotted the capacity curves of two benchmark schemes, i.e., 2-by-2 MIMO scheme without using graphene and the single-input single-output (SISO) scheme using graphene.

Fig. 4 shows the instantaneous maximum MIMO capacity of our graphene-based MIMO scheme, employing ($M = 2$) transmit and ($N = 2$) plasmonic nano-receivers. The system parameters were the same as those used in Fig. 3(a), i.e., the chemical potential was 0.3 eV, and the spacing D between the plasmonic nano-transmitters/receivers was set to $D = 201$ nm. We also plotted the capacity curve of two benchmark schemes, i.e., the 2-by-2 MIMO scheme without using graphene and the single-input single-output (SISO) scheme using graphene. Observe in Fig. 4 that the proposed 2-by-2 graphene-based MIMO scheme achieved twice higher maximum capacity than that of the single-transmitter and receiver counterpart; this is one of the explicit benefits of the spatial-multiplexing MIMO technique.[2] In contrast, the capacity curve associated with the 2-by-2 MIMO without using graphene exhibited a low capacity, which was similar to that of the SISO system. This is because the antenna spacing of the benchmark MIMO scheme in free space was as low as $D/\lambda_0 = 0.02$ wavelength due to the absence of SPPs, and hence it had a significantly high correlation.

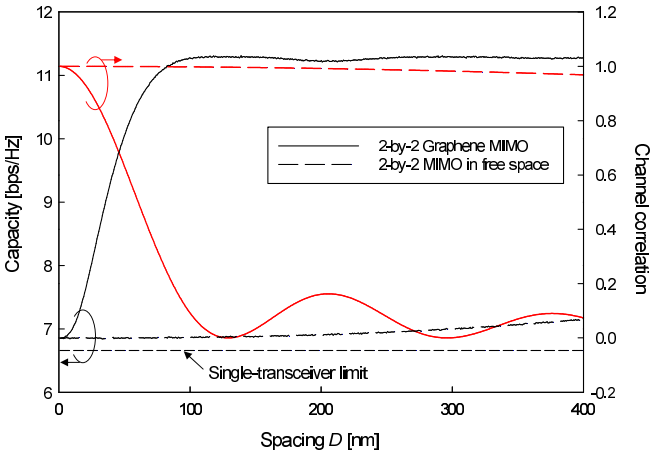

FIGURE 5. Comparisons of the capacity and the channel correlation of our graphene MIMO with those of the conventional free-space MIMO systems, as functions of the spacing between two plasmonic nano transmiters (receivers). The SNR value was 20 dB. (black lines: capacity, red lines: channel correlation.)

Fig. 5 shows the effects of transmitter (receiver) spacing D on the capacity limit at the received SNR = 20 dB, while also plotting the value of the channel correlation. Here, we assumed for simplicity that the distance D between the ($M = 2$) plasmonic nano-sources was equal to that of the ($N = 2$) plasmonic nano-receivers, and hence the channel correlation in Fig. 5 corresponds to either the transmitters or the receivers. Moreover, in the simulations we used the theoretical correlated Rayleigh fading channels according to [23]. It can be seen in Fig. 5 that upon increasing the transmitter (receiver) spacing D, the capacity of our graphene-based MIMO scheme is considerably increased until it approaches the expected capacity at around $D = 100$ nm. By contrast, the capacity of the conventional free-space MIMO system remained close to that of a single-transceiver. This is because the SPP effects of the proposed scheme allowed us to achieve a wavelength that was approximately 30 times shorter, hence resulting in low correlation between the plasmonic nano-transmitters (receivers).

In our simulations, we assumed ideal point sources for the plasmonic nano-transmitters. This assumption allowed us to focus our attention on the demonstration of the novel nanoscale MIMO concept using the graphene propagation channel. Hence, our novel finding is not limited to a specific

[2]In order to provide further insight, these benefits were achieved owing to the exclusive properties of graphene channel, i.e., a low-loss propagation and a high reflection coefficient, as above mentioned. These two properties enabled us to attain an effective multipath rich environment at each plasmonic nano-receiver, which is beneficial for MIMO communications.

antenna array configuration, but is readily applicable to any types of nanoscale antenna systems. For example, the existing nanoantennas [3], [7] would be promising candidates. The potential efficiency loss of a plasmonic nanoantenna element typically reduces the channel capacity shown in Fig. 4, resulting in a simple leftward shift of the capacity curve. Additionally, coupling between the plasmonic nanoatenna elements in free space may increase the channel correlation and reduce the channel capacity. The more elaborate development of such antenna arrays is an open issue.

V. CONCLUSIONS

In this paper, we proposed a graphene-based MIMO, which is capable of combating the conventional MIMO's essential limitations regarding spacing between individual plasmonic nano-transmitters (receivers). One of the benefits of using graphene is that by varying its chemical potential, the received power of the MIMO receiver may be increased. Our simulation results demonstrated that at a frequency of 10 THz, the MIMO transceiver size is approximately 30 times smaller than that required by conventional methods.

REFERENCES

[1] H. G. Craighead, "Nanoelectromechanical systems," *Science*, vol. 290, no. 5496, pp. 1532–1535, 2000.
[2] I. F. Akyildiz, F. Brunetti, and C. Blázquez, "Nanonetworks: A new communication paradigm," *Comput. Netw.*, vol. 52, no. 12, pp. 2260–2279, 2008.
[3] A. Alù and N. Engheta, "Wireless at the nanoscale: Optical interconnects using matched nanoantennas," *Phys. Rev. Lett.*, vol. 104, no. 21, p. 213902, 2010.
[4] I. F. Akyildiz and J. M. Jornet, "Electromagnetic wireless nanosensor networks," *Nano Commun. Netw.*, vol. 1, no. 1, pp. 3–19, Mar. 2010.
[5] T. Nakano, M. J. Moore, F. Wei, A. V. Vasilakos, and J. Shuai, "Molecular communication and networking: Opportunities and challenges," *IEEE Trans. Nanobiosci.*, vol. 11, no. 2, pp. 135–148, Jun. 2012.
[6] A. Vakil and N. Engheta, "Transformation optics using graphene," *Science*, vol. 332, no. 6035, pp. 1291–1294, 2011.
[7] P. J. Burke, S. Li, and Z. Yu, "Quantitative theory of nanowire and nanotube antenna performance," *IEEE Trans. Nanotechnol.*, vol. 5, no. 4, pp. 314–334, Jul. 2006.
[8] C. Rutherglen and P. Burke, "Carbon nanotube radio," *Nano Lett.*, vol. 7, no. 11, pp. 3296–3299, 2007.
[9] K. Jensen, J. Weldon, H. Garcia, and A. Zettl, "Nanotube radio," *Nano Lett.*, vol. 7, no. 11, pp. 3508–3511, 2007.
[10] Z. L. Wang, "Towards self-powered nanosystems: From nanogenerators to nanopiezotronics," *Adv. Funct. Mater.*, vol. 18, no. 22, pp. 3553–3567, Nov. 2008.
[11] Y. Ouyang, Y. Yoon, J. K. Fodor, and J. Guo, "Comparison of performance limits for carbon nanoribbon and carbon nanotube transistors," *Appl. Phys. Lett.*, vol. 89, no. 20, p. 203107, 2006.
[12] L. A. Ponomarenko *et al.*, "Chaotic dirac billiard in graphene quantum dots," *Science*, vol. 320, no. 5874, pp. 356–358, 2008.
[13] K. S. Novoselov *et al.*, "Electric field effect in atomically thin carbon films," *Science*, vol. 306, no. 5696, pp. 666–669, 2004.
[14] F. H. L. Koppens, D. E. Chang, and F. J. G. de Abajo, "Graphene plasmonics: A platform for strong light–matter interactions," *Nano Lett.*, vol. 11, no. 8, pp. 3370–3377, Jul. 2011.
[15] Y. Yao *et al.*, "Broad electrical tuning of graphene-loaded plasmonic antennas," *Nano Lett.*, vol. 13, no. 3, pp. 1257–1264, Feb. 2013.
[16] J. M. Jornet and I. F. Akyildiz, "Graphene-based plasmonic nano-antenna for terahertz band communication in nanonetworks," *IEEE J. Sel. Areas Commun.*, vol. 31, no. 12, pp. 685–694, Dec. 2013.
[17] Y. Huang, L.-S. Wu, M. Tang, and J. Mao, "Design of a beam reconfigurable THz antenna with graphene-based switchable high-impedance surface," *IEEE Trans. Nanotechnol.*, vol. 11, no. 4, pp. 836–842, Jul. 2012.
[18] L. L. Hanzo, O. Alamri, M. El-Hajjar, and N. Wu, *Near-Capacity Multi-Functional MIMO Systems: Sphere-Packing, Iterative Detection and Cooperation*. New York, NY, USA: Wiley, 2009.
[19] S. Sugiura, S. Chen, and L. Hanzo, "MIMO-aided near-capacity turbo transceivers: Taxonomy and performance versus complexity," *IEEE Commun. Surveys Tuts.*, vol. 14, no. 2, pp. 421–442, May 2012.
[20] D. Gesbert, M. Shafi, D.-S. Shiu, P. J. Smith, and A. Naguib, "From theory to practice: An overview of MIMO space-time coded wireless systems," *IEEE J. Sel. Areas Commun.*, vol. 21, no. 3, pp. 281–302, Apr. 2003.
[21] Q. Li *et al.*, "MIMO techniques in WiMAX and LTE: A feature overview," *IEEE Commun. Mag.*, vol. 48, no. 5, pp. 86–92, May 2010.
[22] P.-S. Kildal and K. Rosengren, "Correlation and capacity of MIMO systems and mutual coupling, radiation efficiency, and diversity gain of their antennas: Simulations and measurements in a reverberation chamber," *IEEE Commun. Mag.*, vol. 42, no. 12, pp. 104–112, Dec. 2004.
[23] A. Paulraj, R. Nabar, and D. Gore, *Introduction to Space-Time Wireless Communications*. Cambridge, U.K.: Cambridge Univ. Press, 2003.
[24] G. Lerosey, J. de Rosny, A. Tourin, and M. Fink, "Focusing beyond the diffraction limit with far-field time reversal," *Science*, vol. 315, no. 5815, pp. 1120–1122, 2007.
[25] Z. Xu, X. Dong, and J. Bornemann, "Spectral efficiency of carbon nanotube antenna based MIMO systems in the terahertz band," *IEEE Wireless Commun. Lett.*, vol. 2, no. 6, pp. 631–634, Dec. 2013.
[26] S. Sugiura, S. Chen, and L. Hanzo, "A universal space-time architecture for multiple-antenna aided systems," *IEEE Commun. Surveys Tuts.*, vol. 14, no. 2, pp. 401–420, May 2012.
[27] L. Hanzo, H. Haas, S. Imre, D. O'Brien, M. Rupp, and L. Gyongyosi, "Wireless myths, realities, and futures: From 3G/4G to optical and quantum wireless," *Proc. IEEE*, vol. 100, no. 13, pp. 1853–1888, May 2012.
[28] P. W. Wolniansky, G. J. Foschini, G. D. Golden, and R. Valenzuela, "V-BLAST: An architecture for realizing very high data rates over the rich-scattering wireless channel," in *Proc. Int. Symp. Signals, Syst., Electron. (ISSSE)*, Pisa, Italy, Sep./Oct. 1998, pp. 295–300.
[29] G. J. Foschini and M. J. Gans, "On limits of wireless communications in a fading environment when using multiple antennas," *Wireless Pers. Commun.*, vol. 6, no. 3, pp. 311–335, 1998.
[30] A. Goldsmith, S. A. Jafar, N. Jindal, and S. Vishwanath, "Capacity limits of MIMO channels," *IEEE J. Sel. Areas Commun.*, vol. 21, no. 5, pp. 684–702, Jun. 2003.
[31] A. F. Molisch, M. Steinbauer, M. Toeltsch, E. Bonek, and R. S. Thoma, "Capacity of MIMO systems based on measured wireless channels," *IEEE J. Sel. Areas Commun.*, vol. 20, no. 3, pp. 561–569, Apr. 2002.
[32] M. A. Jensen and J. W. Wallace, "A review of antennas and propagation for MIMO wireless communications," *IEEE Trans. Antennas Propag.*, vol. 52, no. 11, pp. 2810–2824, Nov. 2004.
[33] C. Waldschmidt, S. Schulteis, and W. Wiesbeck, "Complete RF system model for analysis of compact MIMO arrays," *IEEE Trans. Veh. Technol.*, vol. 53, no. 3, pp. 579–586, May 2004.
[34] A. S. Y. Poon, R. W. Brodersen, and D. N. C. Tse, "Degrees of freedom in multiple-antenna channels: A signal space approach," *IEEE Trans. Inf. Theory*, vol. 51, no. 2, pp. 523–536, Feb. 2005.
[35] V. Jungnickel, V. Pohl, and C. von Helmolt, "Capacity of MIMO systems with closely spaced antennas," *IEEE Commun. Lett.*, vol. 7, no. 8, pp. 361–363, Aug. 2003.
[36] B. K. Lau, J. B. Andersen, G. Kristensson, and A. F. Molisch, "Impact of matching network on bandwidth of compact antenna arrays," *IEEE Trans. Antennas Propag.*, vol. 54, no. 11, pp. 3225–3238, Nov. 2006.
[37] B. N. Getu and J. B. Andersen, "The MIMO cube—A compact MIMO antenna," *IEEE Trans. Wireless Commun.*, vol. 4, no. 3, pp. 1136–1141, May 2005.
[38] D. W. Browne, M. Manteghi, M. P. Fitz, and Y. Rahmat-Samii, "Experiments with compact antenna arrays for MIMO radio communications," *IEEE Trans. Antennas Propag.*, vol. 54, no. 11, pp. 3239–3250, Nov. 2006.
[39] M. M. Bait-Suwailam, M. S. Boybay, and O. M. Ramahi, "Electromagnetic coupling reduction in high-profile monopole antennas using single-negative magnetic metamaterials for MIMO applications," *IEEE Trans. Antennas Propag.*, vol. 58, no. 9, pp. 2894–2902, Sep. 2010.
[40] J. Lee, Y.-K. Hong, S. Bae, G. S. Abo, W.-M. Seong, and G.-H. Kim, "Miniature long-term evolution (LTE) MIMO ferrite antenna," *IEEE Antennas Wireless Propag. Lett.*, vol. 10, pp. 603–606, 2011.
[41] B. K. Lau and J. B. Andersen, "Simple and efficient decoupling of compact arrays with parasitic scatterers," *IEEE Trans. Antennas Propag.*, vol. 60, no. 2, pp. 464–472, Feb. 2012.

[42] C. Volmer, J. Weber, R. Stephan, K. Blau, and M. A. Hein, "An eigen-analysis of compact antenna arrays and its application to port decoupling," *IEEE Trans. Antennas Propag.*, vol. 56, no. 2, pp. 360–370, Feb. 2008.
[43] R. Gordon, "Surface plasmon nanophotonics: A tutorial," *IEEE Nanotechnol. Mag.*, vol. 2, no. 3, pp. 12–18, Sep. 2008.
[44] W. L. Barnes, A. Dereux, and T. W. Ebbesen, "Surface plasmon subwavelength optics," *Nature*, vol. 424, no. 6950, pp. 824–830, 2003.
[45] K. S. Novoselov *et al.*, "Two-dimensional gas of massless Dirac fermions in graphene," *Nature*, vol. 438, no. 7065, pp. 197–200, 2005.
[46] Y. Zhang, Y.-W. Tan, H. L. Stormer, and P. Kim, "Experimental observation of the quantum Hall effect and Berry's phase in graphene," *Nature*, vol. 438, no. 7065, pp. 201–204, 2005.
[47] K. I. Bolotin *et al.*, "Ultrahigh electron mobility in suspended graphene," *Solid State Commun.*, vol. 146, no. 9, pp. 351–355, 2008.
[48] M. Jablan, H. Buljan, and M. Soljačić, "Plasmonics in graphene at infrared frequencies," *Phys. Rev. B*, vol. 80, no. 24, p. 245435, 2009.
[49] M. Liu *et al.*, "A graphene-based broadband optical modulator," *Nature*, vol. 474, no. 7349, pp. 64–67, 2011.
[50] M. Liu, X. Yin, and X. Zhang, "Double-layer graphene optical modulator," *Nano Lett.*, vol. 12, no. 3, pp. 1482–1485, 2012.
[51] F. Schwierz, "Graphene transistors," *Nature Nanotechnol.*, vol. 5, no. 7, pp. 487–496, 2010.
[52] L. Liao *et al.*, "Scalable fabrication of self-aligned graphene transistors and circuits on glass," *Nano Lett.*, vol. 12, no. 6, pp. 2653–2657, 2011.
[53] F. Xia, T. Mueller, Y.-M. Lin, A. Valdes-Garcia, and P. Avouris, "Ultrafast graphene photodetector," *Nature Nanotechnol.*, vol. 4, no. 12, pp. 839–843, 2009.
[54] T. Mueller, F. Xia, and P. Avouris, "Graphene photodetectors for high-speed optical communications," *Nature Photon.*, vol. 4, no. 5, pp. 297–301, 2010.
[55] X. Wang, Z. Cheng, K. Xu, H. K. Tsang, and J.-B. Xu, "High-responsivity graphene/silicon-heterostructure waveguide photodetectors," *Nature Photon.*, vol. 7, pp. 888–891, Sep. 2013.
[56] L. A. Falkovsky, "Optical properties of graphene," *J. Phys., Conf. Ser.*, 2008, vol. 129, no. 1, p. 012004.
[57] J. Chen *et al.*, "Optical nano-imaging of gate-tunable graphene plasmons," *Nature*, vol. 487, pp. 77–81, Jul. 2012.
[58] J. Chen *et al.*, "Strong plasmon reflection at nanometer-size gaps in monolayer graphene on SiC," *Nano Lett.*, vol. 13, no. 12, pp. 6210–6215, 2013.
[59] J. L. Garcia-Pomar, A. Y. Nikitin, and L. Martin-Moreno, "Scattering of graphene plasmons by defects in the graphene sheet," *ACS Nano*, vol. 7, no. 6, pp. 4988–4994, 2013.
[60] Z. Fei *et al.*, "Electronic and plasmonic phenomena at graphene grain boundaries," *Nature Nanotechnol.*, vol. 8, pp. 821–825, Oct. 2013.
[61] H. J. Xu, W. B. Lu, Y. Jiang, and Z. G. Dong, "Beam-scanning planar lens based on graphene," *Appl. Phys. Lett.*, vol. 100, no. 5, p. 051903, 2012.
[62] M. Kadic, S. Guenneau, S. Enoch, and S. A. Ramakrishna, "Plasmonic space folding: Focusing surface plasmons *via* negative refraction in complementary media," *ACS Nano*, vol. 5, no. 9, pp. 6819–6825, 2011.
[63] *CST Microwave Studio Manual*, Darmstadt, Germany. (2013). [Online]. Available: http://www.cst.com
[64] D. Mann, A. Javey, J. Kong, Q. Wang, and H. Dai, "Ballistic transport in metallic nanotubes with reliable Pd ohmic contacts," *Nano Lett.*, vol. 3, no. 11, pp. 1541–1544, 2003.
[65] P. Li and T. Taubner, "Broadband subwavelength imaging using a tunable graphene-lens," *ACS Nano*, vol. 6, no. 11, pp. 10107–10114, 2012.
[66] H. Ditlbacher *et al.*, "Silver nanowires as surface plasmon resonators," *Phys. Rev. Lett.*, vol. 95, no. 25, p. 257403, Dec. 2005.

SHINYA SUGIURA (M'06–SM'12) received the B.S. and M.S. degrees in aeronautics and astronautics from Kyoto University, Kyoto, Japan, in 2002 and 2004, respectively, and the Ph.D. degree in electronics and electrical engineering from the University of Southampton, Southampton, U.K., in 2010.

He was a Research Scientist with Toyota Central Research and Development Laboratories, Inc., Nagakute, Japan, from 2004 to 2012. Since 2013, he has been an Associate Professor with the Department of Computer and Information Sciences, Tokyo University of Agriculture and Technology, Tokyo, Japan, where he heads the Wireless Communications Research Group. His research has covered a range of areas in wireless communications, networking, signal processing, and antenna design. He has authored or co-authored over 60 refereed research publications, including 35 IEEE journal and magazine papers.

Dr. Sugiura was a recipient of numerous awards, including the 28th Telecom System Technology Award from the Telecommunications Advancement Foundation in 2013, the 6th IEEE Communications Society Asia-Pacific Outstanding Young Researcher Award in 2011, the 13th Ericsson Young Scientist Award in 2011, and the 2008 IEEE Antennas and Propagation Society Japan Chapter Young Engineer Award. He was also certified as an Exemplary Reviewer of the IEEE COMMUNICATIONS LETTERS in 2013 and 2014.

HIDEO IIZUKA (M'04) received the B.S. and M.S. degrees in electrical engineering from Saitama University, Saitama, Japan, in 1995 and 1997, respectively, and the Ph.D. degree in engineering from the Nagoya Institute of Technology, Nagoya, Japan, in 2007.

He joined Toyota Central Research and Development Laboratories, Inc., Nagakute, Japan, in 1997. He was a Visiting Scholar with the University of Birmingham, Birmingham, U.K., from 2001 to 2002, and the Toyota Research Institute, Toyota Motor Engineering and Manufacturing North America, Inc., Ann Arbor, MI, USA, from 2008 to 2011. His research interests include the analysis and development of electromagnetic devices and systems for automotive applications.

Dr. Iizuka was a recipient of the IEICE Young Engineering Award in 2001.